

Transport in random quantum dot superlattices

I. Gómez, F. Domínguez-Adame and E. Diez

GISC, Departamento de Física de Materiales, Universidad Complutense, E-28040 Madrid, Spain

P. Orellana

Departamento de Física, Universidad Católica del Norte, Casilla 1280, Antofagasta, Chile

(February 1, 2008)

Abstract

We present a novel model to calculate single-electron states in random quantum dot superlattices made of wide-gap semiconductors. The source of disorder comes from the random arrangement of the quantum dots (configurational disorder) as well as spatial inhomogeneities of their shape (morphological disorder). Both types of disorder break translational symmetry and prevent the formation of minibands, as occurs in regimented arrays of quantum dots. The model correctly describes channel mixing and broadening of allowed energy bands due to elastic scattering by disorder.

I. INTRODUCTION

Latest advances in nanotechnology make it possible to growth quantum dot (QD) superlattices [1,2]. In view of the analogy between atoms and QDs, it is expected that strongly confined levels overlap when QDs are closely packed. Although this analogy cannot be complete since carriers in QDs are influenced by phonons, defects and interface states, the resulting collective levels will depend on the particular arrangement of QDs. In this sense, QD arrays grown by molecular beam epitaxy can be completely random [3,4], partially regimented [1,2] or may be regularly stacked (high regimentation) [5]. Electronic states in highly regimented QDs are adequately described within envelope-function approximation with a three dimensional Kronig-Penney model and the occurrence of miniband have been established [6]. However, the lack of periodicity observed in random QDs superlattices demands different approaches.

In the present work we introduce a two-dimensional effective-mass model to study the effects of scattering by disorder on electron transmission through random quantum-dots superlattices. To this end, the Ben Daniel-Duke equation is discretized, boundary conditions are discussed and scattering solutions are found by means of the transfer-matrix method for *any* arbitrary array of QDs. The model is worked out in a two-dimensional space for computational limitations, although it will be clear that generalization to three dimensions is rather straightforward. Finally, we present the numerical results for the transmission coefficient through random arrays of coupled QDs and the main conclusions of the work.

II. MODEL

We consider the Ben Daniel-Duke equation with constant effective mass m^* at the Γ valley for the electron envelope function $\chi(y, z)$. In order to find numerically the single electron states, the whole sample is divided into three different regions, namely left (I) and right (III) contacts and the random QDs (II), where scattering by disorder takes place. Figure 1 shows a schematic view of the three spatial regions. We then consider a mesh with lattice spacings a_y and a_z in the y and z directions, respectively. Defining $t_y \equiv -\hbar^2/(2m^*a_y^2)$ and $t_z \equiv -\hbar^2/(2m^*a_z^2)$, we obtain the following discrete effective-mass equation

$$t_z(\chi_{n+1,m} + \chi_{n-1,m}) + t_y(\chi_{n,m+1} + \chi_{n,m-1}) + (U_{n,m} - 2t_z - 2t_y)\chi_{n,m} = E\chi_{n,m}. \quad (1)$$

The potential term $U_{n,m}$ in Eq. (1) is given by the conduction-band edge energy at the point (na_y, ma_z) . Therefore, disorder enters the equation through this diagonal term. Contacts are characterized by flat band conditions, $U(n, m) = 0$, in the absence of applied electric field. Clearly, the effects of the applied field can be easily taken into account within the present approach by adding a linearly varying potential of the form $U_F(n, m) = -eFma_z$, F being the applied field.

III. TRANSFER MATRIX FORMALISM

In order to solve the tight binding-like equation (1) we use the transfer matrix method based on the solutions calculated for each slide of the system along the z direction. For

the sake of simplicity in the calculation, we define $\vec{\phi}_n$ ($n = 0, 1, \dots, N + 1$) as a vector whose components are $\phi_n^m \equiv \chi_{n,m}$ ($m=1, \dots, M$). Here M and $N + 1$ are the number of mesh divisions in the y and z directions, respectively. Thus, Eq. (1) can be cast in a more compact form

$$\begin{pmatrix} \vec{\phi}_{n-1} \\ \vec{\phi}_n \end{pmatrix} = \begin{pmatrix} t_z^{-1}(E\mathcal{I} - \mathcal{M}_n) & -\mathcal{I} \\ \mathcal{I} & \mathcal{O} \end{pmatrix} \begin{pmatrix} \vec{\phi}_n \\ \vec{\phi}_{n+1} \end{pmatrix}, \quad (2)$$

where \mathcal{I} and \mathcal{O} are the $M \times M$ identity and null matrices respectively. The matrix \mathcal{M}_n splits into the form $\mathcal{M}_n = \mathcal{R}_n + \mathcal{B}_n$. The diagonal elements of the tridiagonal matrix \mathcal{R}_n are $(\mathcal{R}_n)_{mm} = U_{n,m} - 2t_z - 2t_y$ while nonvanishing off-diagonal elements equal t_y . The matrix \mathcal{B}_n depends on the boundary conditions to be specified later.

We can obtain the expression of the envelope function amplitudes in the left contact as a function of the amplitudes in the right one

$$\begin{pmatrix} \vec{\phi}_0 \\ \vec{\phi}_1 \end{pmatrix} = \mathcal{T}^{(N)} \begin{pmatrix} \vec{\phi}_N \\ \vec{\phi}_{N+1} \end{pmatrix}, \quad \mathcal{T}^{(N)} \equiv \prod_{n=1}^N \begin{pmatrix} t_z^{-1}(E\mathcal{I} - \mathcal{M}_n) & -\mathcal{I} \\ \mathcal{I} & \mathcal{O} \end{pmatrix}, \quad (3)$$

where $\mathcal{T}^{(N)}$ is the transfer matrix for the heterostructure.

IV. SCATTERING SOLUTIONS

The envelope functions within the contacts will be determined by the boundary conditions. These boundary conditions are open in the z direction, and periodic on each slide, namely in the y direction. Consequently, all elements of \mathcal{R}_n vanish except $(\mathcal{R}_n)_{1M} = (\mathcal{R}_n)_{M1} = t_y$. The former conditions imply plane wave solutions in the z axis, and the latter yield an energy discretization on y . As a consequence, this discretization results in a number of transverse channels equal to the number of points in the transverse mesh direction. Considering $U_{n,m}$ to be constant at the contacts, that is, considering perfect leads so no voltage drop occurs within regions I and III, and setting $\chi_{n,1} = \chi_{n,M+1}$, a particular solution of Eq. (1) is given by

$$\begin{aligned} \chi_{n,m}^l = & \frac{1}{\sqrt{\mathcal{N}_l}} \exp\left(i \frac{2\pi l}{M} m\right) \exp(ik_l a_z n) \\ & + \sum_{j=1}^M \hat{r}_{lj} \frac{1}{\sqrt{\mathcal{N}_j}} \exp\left(i \frac{2\pi j}{M} m\right) \exp(-ik_j a_z n), \quad (m, n) \in \text{I}. \end{aligned} \quad (4a)$$

at the left contact while at the right contact we have

$$\chi_{n,m}^l = \sum_{j=1}^M \hat{t}_{lj} \frac{1}{\sqrt{\mathcal{N}_j}} \exp\left(i \frac{2\pi j}{M} m\right) \exp(ik_j a_z n), \quad (m, n) \in \text{III}. \quad (4b)$$

where the normalization constant is chosen to ensure that all the *propagating* modes carry the same current

$$\mathcal{N}_j = \frac{1}{a_y^2} \sin^2\left(\frac{2\pi j}{M}\right) + \frac{1}{a_z^2} \sin^2(k_j a_z)$$

and

$$k_j = \frac{1}{a_z} \cos^{-1} \left\{ \frac{1}{2t_z} \left[E - 2t_y \left(\cos \frac{2\pi j}{M} - 1 \right) \right] + 1 \right\}.$$

These expressions remain valid for an applied electric field F provided the electronic momentum k_j is substituted within region *III* in the following way

$$\begin{aligned} k_j &\leftrightarrow q_j \\ q_j &= \frac{1}{a_z} \cos^{-1} \left\{ \frac{1}{2t_z} \left[E + eV - 2t_y \left(\cos \frac{2\pi j}{M} - 1 \right) \right] + 1 \right\}. \end{aligned} \quad (5)$$

Here $V = FL$, where L is the length of region *II*.

The matrices \hat{r} and \hat{t} appearing in equations (4a) and (4b) are the *reflection* and *transmission* matrices and they are responsible for the channel *mixing* due to scattering events. Thus, \hat{r}_{ij} represents the probability amplitude for an electron impinging in channel i to be reflected into the channel j . Note that the solution within region *II* is unknown. Actually, we are not interested in this solution since all the physics of the scattering problem is contained in the *mixing* matrices \hat{t} and \hat{r} . In particular, we can compute the conductance. From the Landauer-Büttiker formalism [7], the zero temperature two-leads multichannel conductance can be calculated using de Fisher-Lee formula [8]

$$G = \frac{2e^2}{h} \text{Tr}(\hat{t}^\dagger \hat{t}), \quad (6)$$

where Tr stands for the trace of the matrix.

V. CONFIGURATIONAL AND MORPHOLOGICAL DISORDER

In order to describe epitaxially random QD superlattices, we consider they are arranged on a nonregular lattice (configurational disorder). But, in addition, there exists another source of disorder due to spatial inhomogeneities that make the shape to be slightly different (morphological disorder). To mimic both types of disorder we assume an array of rectangular QDs, randomly displaced from the regular lattice sites, whose size also change randomly from dot to dot (see Fig. 1). To avoid the profusion of free parameters, we consider that the energy of the confinement potential ΔE_c provided by the high bandgap semiconductor is the same for every QD. This is not a serious shortcoming since spatial inhomogeneities of the conduction-band offset and fluctuations of individual QDs shapes yield essentially the same results. In addition, our model could easily deal with nonconstant values of ΔE_c if further improvements are required.

We will separate the effects of configurational and morphological disorder for the sake of clarity. Configurational disorder means that every QD shifts its position $\delta \mathbf{r} = (\delta y, \delta z)$ while its size $d_y \times d_z$ remains unchanged (see Fig. 2). Here δy and δz are random uncorrelated variables with zero mean and distributed according to box probability functions of width W_y and W_z , respectively. To simulate the change of the shape (morphological disorder) we consider that the QD is enlarged along the Z axis an amount $\delta \zeta$ while its center stays on a regular lattice (see Fig. 2), where $\delta \zeta$ is uniformly distributed with zero mean and width W_ζ .

VI. RESULTS

As a working example, we have performed several numerical calculations in order to study the effect of both configurational and morphological disorder over the conductance of random QDs superlattices made of GaAs-In_xGa_{1-x}As heterojunctions. We have considered regimented and disordered 4×4 arrays of QDs to elucidate the effects of randomness. The conduction-band offset, ΔE_c , is taken to be 70% of the difference of the gaps ΔE_g in strained GaAs-In_xGa_{1-x}As heterojunctions, where $\Delta E_g = 1.45x$ eV. For definiteness we set $x = 0.35$ and consequently $\Delta E_c = 0.35$ eV. In addition, since we are mainly interested in the effects of the coupling between the QDs through the high bandgap semiconductor rather in the confined levels of individual QD, we have taken $m^* = 0.067$ in units of the bare electron mass, corresponding to the embedding semiconductor. Let us mention that the model can be easily generalized to include a different effective mass inside the QDs. The size of the regimented QDs is $d_y \times d_z$ with $d_y = 8.0$ nm and $d_z = 1.6$ nm. The separation between centers in the regimented array is 14.0 and 6.8 nm along the Y and Z axes, respectively. The number of mesh points along the two spatial directions are $M = 50$ and $N + 1 = 39$.

As typical results of our simulations, Fig. 3 shows the conductance versus Fermi energy, measured from the conduction-band edge in In_xGa_{1-x}As, in the absence of applied field. Solid line corresponds to regimented QDs. The coupling between the QDs splits the energy levels and results in the formation of minibands [6]. From Fig. 3 we observe the occurrence of two well-defined minibands below the barrier when disorder is absent, in agreement with previous results [6]. Each band is characterized by four main conductance peaks and each peak is the convolution of four peaks that cannot be resolved except for the lower one in the higher miniband (see inset of Fig. 3).

Transport through the miniband changes as soon as some degree of randomness is considered in the model, as expected. Mean size and separation between QDs as well as fluctuations around those values strongly depend on the growth conditions (e.g. growth temperature) and subsequent thermal treatments [4]. As an example, Fig. 3 shows the conductance for configurational ($W_y = 2.0$ nm and $W_z = 1.2$ nm) and morphological ($W_\zeta = 0.8$ nm) disorder, obtained by averaging over 100 realizations of the disorder. As a main point, we notice that electronic states in the array of random QDs behaves like an amorphous material since the conductance strongly decreases while the allowed energies broadens due to the fluctuations of QD energy levels for each realization of the disorder.

Concerning the effects of a uniform applied electric field, we have computed the conductance for a given Fermi energy ($E = 0.27$ eV) as a function of the applied bias V . The potential was assumed to drop uniformly across region II. Figure 4 shows the conductance versus applied bias for regimented as well as random QD superlattices. Regimented QD superlattices present three well-defined negative dG/dV regions due to resonant tunneling through the QDs. The observed peak-to-valley ratios become worse as soon as disorder is included in the calculation, especially in the case of configurational disorder.

VII. CONCLUSIONS

In summary, we have presented a method to study electron transport through random QD superlattices. The method is based on the transfer matrix formalism applied to the

discrete Ben Daniel-Duke Hamiltonian for the electron envelope function. A careful analysis of the scattering solutions under appropriate boundary conditions (periodic and open along the lateral and longitudinal directions, respectively) allows us to obtain the two-channel conductance. For regimented QDs (regular array of QDs) the conductance shows clear signatures of the miniband structure, as previously predicted by a Kronig-Penney model for strongly coupled QDs [6]. However, the novelty of the model lies in the fact that random QD superlattices can also be studied. To this end, two models of disorder (configurational and morphological) have been introduced. Disorder reduces the conductance due to Anderson localization of the envelope functions and broadens the allowed energy bands. The characteristic G - V presents several regions of negative dG/dV , although the peak-to-valley ratios strongly decrease due to disorder.

ACKNOWLEDGMENTS

Work in Madrid was supported by DGI-MCyT (Project MAT2000-0734) and CAM (Project 07N/0075/2001). P. Orellana would like to thank Milenio ICM P99-135-F and Cátedra Presidencial de Ciencias for financial support.

REFERENCES

- [1] J. L. Liu, W. G. Wu, A. Balandin, G. L. Jin, and K. L. Wang, Appl. Phys. Lett. **74**, 185 (1999).
- [2] J. L. Liu, W. G. Wu, A. Balandin, G. L. Jin, Y. H. Luo, S. G. Thomas and K. L. Wang, Appl. Phys. Lett. **75**, 1745 (1999).
- [3] I. Tanaka, I. Kamiya, H. Sasaki, N. Qureshi, S. J. Allen, and P. M. Petroff, Appl. Phys. Lett. **74**, 844 (1999).
- [4] P. C. Sharma, K. W. Alt, D. Y. Yeh, and K. L. Wang, Appl. Phys. Lett. **75**, 1273 (1999).
- [5] G. Springholz, V. Holy, M. Pinczolits, and G. Bauer, Science **282**, 734 (1998).
- [6] O. L. Lazarenkova and A. A. Balandin, J. Appl. Phys. **89**, 5509 (2001).
- [7] R. Landauer, IBM J. Res. Dev. **1**, 223 (1957); M. Büttiker, Phys. Rev. Lett. **57**, 1761 (1986); M. Büttiker, IBM J. Res. Dev. **32**, 63 (1988); M. Büttiker, IBM J. Res. Dev. **32**, 317 (1988).
- [8] D. Fisher and P. A. Lee, Phys. Rev. B **23**, 6851 (1981).

FIGURES

FIG. 1. Schematic view of the sample. Regions I and III are the electrical leads of the sample (contacts) and electrons undergo scattering processes only at region II.

FIG. 2. Schematic view of configurational and morphological disorder. In the former case the QD shift its position an amount $\delta\mathbf{r}$ while its nominal size $d_y \times d_z$ remains unchanged. In the later case, the center of the QD does not change while its size along the Z axis increases or decreases an amount $\delta\zeta$.

FIG. 3. Conductance versus energy for a 2D ordered array of 4×4 QDs made of $\text{In}_x\text{Ga}_{1-x}\text{As}$ in GaAs (solid line) with no applied electric field. The inset shows an enlarged view of the lower conductance peak of the second miniband. Results are compared to random 4×4 arrays with configurational (dotted line) and morphological (dashed line) disorder.

FIG. 4. Conductance versus applied bias for a 2D ordered array of 4×4 QDs made of $\text{In}_x\text{Ga}_{1-x}\text{As}$ in GaAs (solid line), when the incoming electron energy is $E = 0.27 \text{ eV}$. Results are compared to random 4×4 arrays with configurational (dotted line) and morphological (dashed line) disorder.

Fig.1, I. Gómez et al.

Self-assembled quantum dots

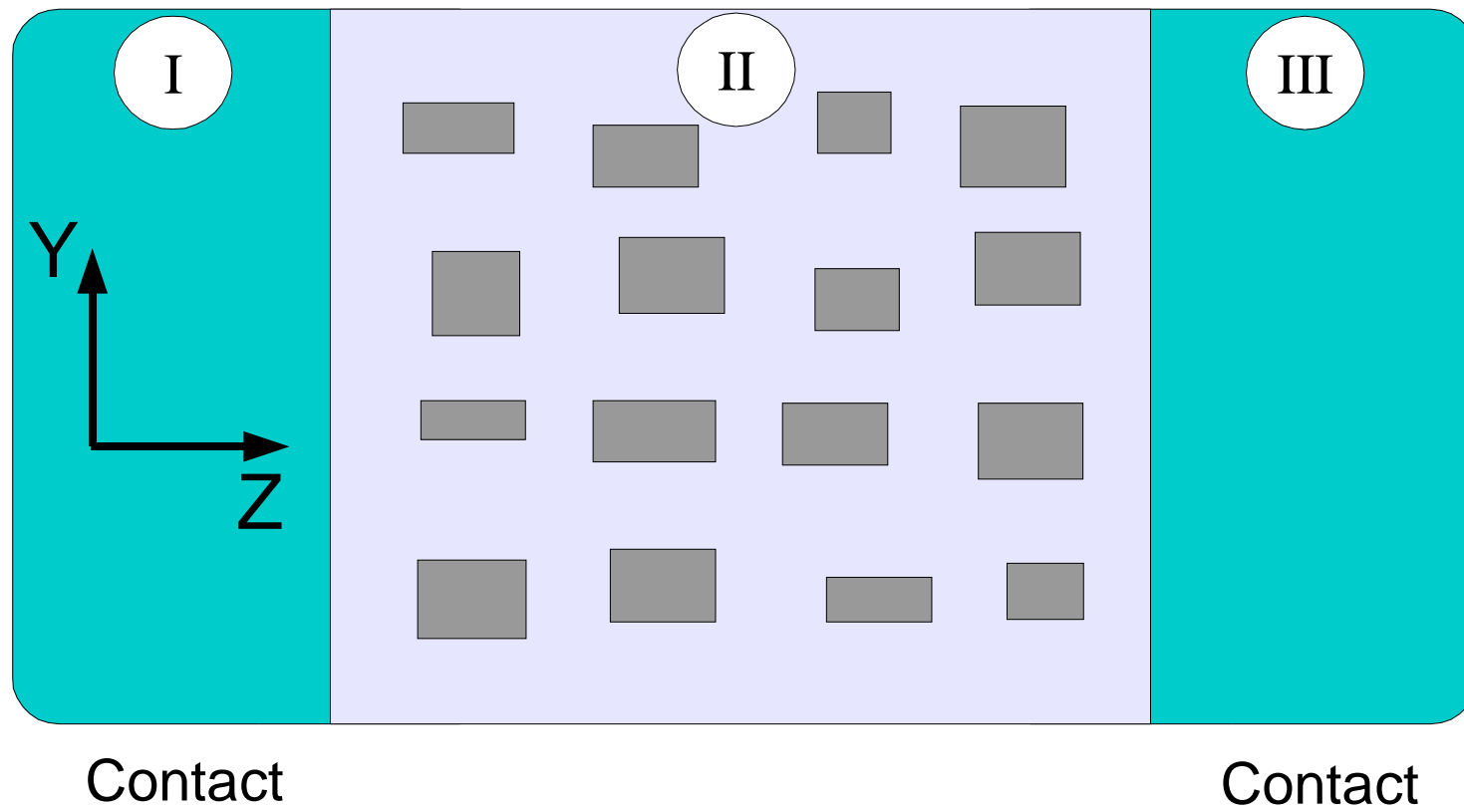


Fig.2, I. Gómez et al.

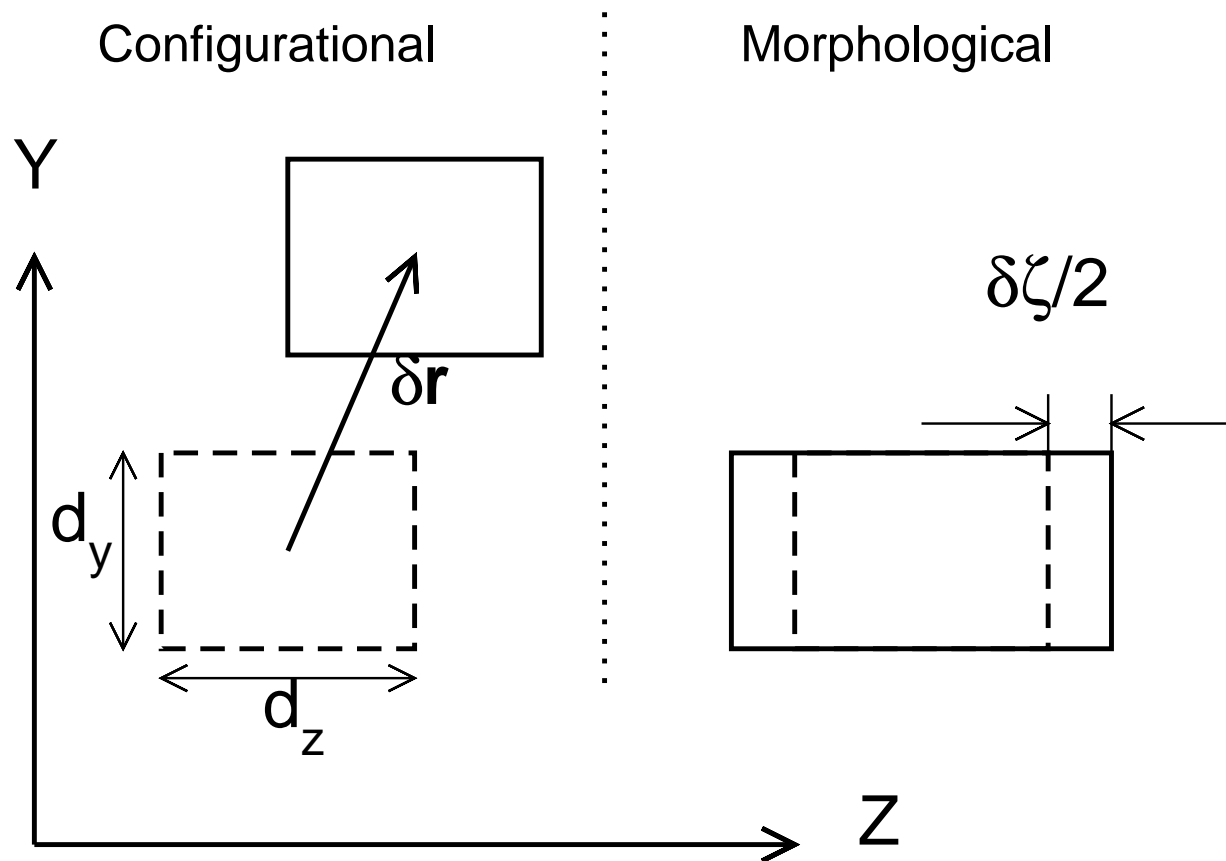


Fig.3, I. Gómez et al.

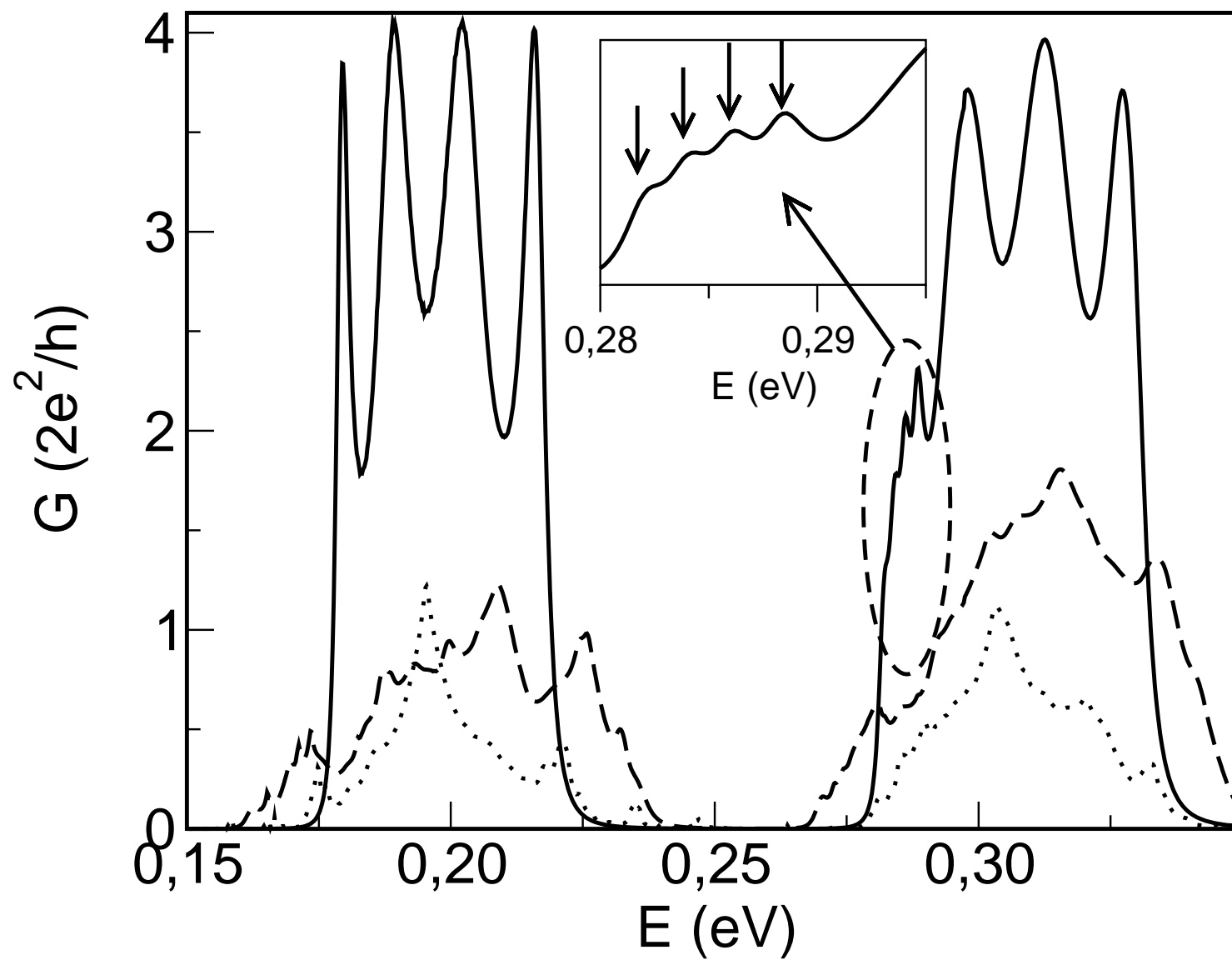


Fig.4, I. Gómez et al.

